nanomaterials

MDPI

Article

Simultaneous Conduction and Valence Band Regulation of Indium-Based Quantum Dots for Efficient H_2 Photogeneration

Xiu-Ping Li †, Rong-Jin Huang †, Cong Chen, Tianduo Li and Yu-Ji Gao *

Shandong Provincial Key Laboratory of Molecular Engineering, School of Chemistry and Chemical Engineering, Qilu University of Technology (Shandong Academy of Science), Jinan 250353, China; lixp2021@163.com (X.-P.L.); huangrongjin2021@163.com (R.-J.H.); chencong199889@163.com (C.C.); ylpt6296@vip.163.com (T.L.)

* Correspondence: yjgao@qlu.edu.cn

† These authors contributed equally to this work.

Abstract: Indium-based chalcogenide semiconductors have been served as the promising candidates for solar H_2 evolution reaction, however, the related studies are still in its infancy and the enhancement of efficiency remains a grand challenge. Here, we report that the photocatalytic H_2 evolution activity of quantized indium chalcogenide semiconductors could be dramatically aroused by the co-decoration of transition metal Zn and Cu. Different from the traditional metal ion doping strategies which only focus on narrowing bandgap for robust visible light harvesting, the conduction and valence band are coordinately regulated to realize the bandgap narrowing and the raising of thermodynamic driving force for proton reduction, simultaneously. Therefore, the as-prepared noble metal-free $Cu_{0.4}$-$ZnIn_2S_4$ quantum dots (QDs) exhibits extraordinary activity for photocatalytic H_2 evolution. Under optimal conditions, the $Cu_{0.4}$-$ZnIn_2S_4$ QDs could produce H_2 with the rate of 144.4 μmol h^{-1} mg^{-1}, 480-fold and 6-fold higher than that of pristine In_2S_3 QDs and Cu-doped In_2S_3 QDs counterparts respectively, which is even comparable with the state-of-the-art cadmium chalcogenides QDs.

Keywords: artificial photosynthesis; bandgap engineering; quantum dots; transition metal doping

Citation: Li, X.-P.; Huang, R.-J.; Chen, C.; Li, T.; Gao, Y.-J. Simultaneous Conduction and Valence Band Regulation of Indium-Based Quantum Dots for Efficient H_2 Photogeneration. *Nanomaterials* **2021**, *11*, 1115. https://doi.org/10.3390/nano11051115

Academic Editor: Antonino Gulino

Received: 8 April 2021
Accepted: 23 April 2021
Published: 26 April 2021

1. Introduction

Artificial photosynthesis is regarded as a promising approach to convert solar energy into usable energy forms, such as molecular hydrogen (H_2), to resolve the energy crisis and environment pollution [1–5]. Hence, synthesis of efficient and low-cost photocatalysts is with vital importance for solar-to-fuel conversion. The semiconductor quantum dots (QDs) which the size is less than their exciton Bohr radius in three dimensions have been attracted tremendous attention in this field owing their unique properties, such as large surface area, abundant surface active sites, multiple exciton generation, short charge transfer distance and so on [6–11]. Among the popular chalcogenide semiconductor-based QDs in artificial photocatalysis, the indium-based chalcogenides seem to be more promising photocatalysts due to their less toxic, noble metal-free as well as the potential visible light harvesting [12–15]. However, the photocatalytic H_2 evolution activity of indium-based photocatalysts is relatively faint so far, especially compared with their cadmium chalcogenide analogs [16–19], so more works remained to be done in optimizing the properties of indium-based QDs. In general, though the bandgap of bulk In_2S_3 (~2.3 eV) is suitable for absorbing visible light, the bandgap of quantized indium chalcogenide nanoparticles is usually larger than 3.0 eV as a result of quantum confinement effect [19–23]. On the other hand, the more negative conduction band edge corresponds to the stronger thermodynamic driving force for proton reduction [24,25], which would result in the higher photocatalytic performance. To balance the above two contradictory effects of narrowing the bandgap and upshifting the conduction band edge, the conduction and valence band should be well designed.

In this contribution, we present that the conduction and valence band edge of indium chalcogenide-based QDs are regulated coordinately by introducing transition metal ions, Zn and Cu. The introduction of Zn ions could level up the conduction band by hybridizing Zn 4s4p and In 5s5p orbitals, while the doping of Cu would form a discrete level from Cu 3d above the valence band of pristine nanocrystals. As the upshift of valence band is obviously larger than that of conduction band, the bandgap of Cu-doped $ZnIn_2S_4$ QDs narrows remarkably to be suitable for absorbing visible light. And the upshift of conduction band by the introduction of Zn resulted in the higher thermodynamic driving force for proton reduction, prominently enhancing the photocatalytic H_2 evolution activity of as-prepared QDs photocatalysts. With the assistance of Ni^{2+} and visible light irradiation, the Cu-doped $ZnIn_2S_4$ QDs could produce H_2 efficiently with the rate of 144.4 μmol h^{-1} mg^{-1}, 480-fold and 6-fold higher than that of pristine In_2S_3 QDs and Cu-doped In_2S_3 QDs, respectively. Under optimal conditions, more than 1000 μmol of H_2 could be produced from 6.0 mL aqueous solution within 16 h irradiation, giving rise to the turnover number (TON) of more than 20260 per QD. The value is even comparable to the cadmium chalcogenide QDs-based photocatalytic systems (Table S1) [6,26]. Further, the apparent quantum yield (AQY) of $Cu_{0.4}$-$ZnIn_2S_4$ QDs could reach 11.8% at 460 nm.

2. Materials and Methods

2.1. Materials

Indium acetate (99.99%), zinc acetate dihydrate (98%), copper(II) acetate monohydrate (99%), L-cysteine (98%), thioacetamide (99%), nickel acetate tetrahydrate (99.9%) and ascorbic acid (H_2A, 99%) were purchased from Alfa Aesar Chemicals Co. Ltd. (Shanghai, China). Other chemicals were of analytical grade without further purification unless otherwise noted. The ultrapure water with 18.2 MΩ cm @ 25 °C was used throughout all the experiments.

2.2. Instruments and Characterizations

UV-vis spectra were measured with a Shimadzu UV-2600PC spectrophotometer (Shimadzu Corp., Kyoto, Japan). Fluorescence measurements were carried out with a Hitachi (model F-4600) spectrophotometer (Hitachi High-Tech Corp., Tokyo, Japan) at room temperature. TEM images were obtained on a JEM 2100 (JEOL Co. Ltd., Tokyo, Japan) operating at 200 kV. X-ray diffraction (XRD) pattern was obtained by using Bruker D8 Focus (Bruker Corp., Billerica, MA, USA) under Cu-K_α radiation. X-ray photoelectron spectroscopy (XPS) measurements were taken on an ESCALAB 250 spectrophotometer (ThermoFisher Scientific Corp., Waltham, MA, USA) with Al-K_α radiation. The binding energy scale was calibrated using the C 1s peak at 284.60 eV. All pH measurements were made with a Model pHS-3C meter (Mettler Toledo FE20, Mettler Toledo (Shanghai) Co. Ltd., Shanghai, China). The generated amount of H_2 was characterized by GC analysis (GC-2014 Shimadzu, Shimadzu Corp., Kyoto, Japan) using N_2 as the carrier gas with a molecular sieve column (5 Å; 30 m × 0.53 mm) and a thermal conductivity detector.

2.3. Synthesis of the Cu-Doped $ZnIn_2S_4$ and In_2S_3 QDs

The indium-based chalcogenides QDs were synthesized through a simple hydrothermal method referring to the previous reported method with some revisions [22]. Taking the $Cu_{0.4}$-$ZnIn_2S_4$ QDs (0.4 represents the precursor molar ratio of Cu with Zn) for example, 0.85 mmol of zinc acetate, 1.70 mmol of indium acetate, 0.34 mmol of copper acetate monohydrate and 3.25 mmol of L-cysteine were dissolved in 30 mL of ultrapure water and adjusted the pH to 9.0. Following this, 3.25 mmol of thioacetamide was added and the mixture was heated to 110 °C for 4 h after vigorous stirring. After reaction, the solution was swiftly cooled to room temperature, and then the product was precipitated and purified with isopropanol and water. The obtained Cu-doped $ZnIn_2S_4$ QDs were dispersed in 40 mL of ultrapure water for further use.

The QDs with different contents of Cu and/or Zn were synthesized by regulating the amount of copper and/or zinc precursors (copper/zinc acetate), while the amount of thioacetamide was also changed with stoichiometric ratio. For the pristine In_2S_3 QDs, the reaction was carried out with the same expect for the absence of copper and zinc precursors.

2.4. General Procedure for Photocatalytic H_2 Evolution

The photocatalytic reactions were performed under 460 nm LEDs irradiation with the Ni^{2+} as cocatalysts and H_2A as the electron donor. Generally, 1.6 mg of QDs, 10 μg of nickel acetate tetrahydrate and 400 mg of ascorbic acid were added to a 20 mL of Pyrex tube. The total reaction volume of the mixture was 6.0 mL by adding ultrapure water and the pH of the solution was adjusted to 5.2 by HCl or NaOH. Prior to irradiation, the sample was sealed and de-aerated by bubbling N_2 for 10 min to remove the dissolved oxygen, and then 1.0 mL of CH_4 was injected the system to serve as internal standard. The amount of evolved H_2 gas was quantified by comparing the area ratio of CH_4 to H_2 and the response factor of CH_4/H_2 in the gas chromatography (GC).

2.5. The Calculated of AQY for $Cu_{0.4}$-$ZnIn_2S_4$ QDs

For the optimal photocatalytic H_2 evolution, the irradiation area was 3.0 cm^2 by 460 nm LEDs (light intensity 100 $mW \cdot cm^{-2}$). The calculation of apparent quantum efficiency (Φ) is according to the following equation:

$$\Phi = \frac{2 \times n_{H_2}}{N} \times 100\%$$

wherein n_{H_2} is the amount of photo-generated H_2 and N is the corresponding amount of incident photon. The amount of incident photon was calculated from the irradiation time, the irradiation area and the illumination power. It showed that about 5.5 mL of H_2 was generated after 1.0 h irradiation. From the combined measurements of the amount of photo-generated H_2 and the corresponding amount of incident photon, the apparent quantum yield was calculated to be 11.8%.

3. Results and Discussion

3.1. Microstructure Characteristics and Composition Analysis

The photocatalysts with different contents of Zn and/or Cu decorated In_2S_3 QDs were synthesized by regulating the species and amount of precursors. According to the photocatalytic H_2 evolution performance, the as-prepared pristine In_2S_3, $ZnIn_2S_4$, $Cu_{0.4}$-In_2S_3 and $Cu_{0.4}$-$ZnIn_2S_4$ QDs were selected for the structure and morphology characterizations. As shown in Figure 1, the diffraction peaks of the pristine In_2S_3 can be indexed as the tetragonal phase In_2S_3 (JCPDS no. 25-0390) [27]. However, though the XRD patterns change clearly after the co-decoration of Zn and Cu ions ($Cu_{0.4}$-$ZnIn_2S_4$), the synthesized counterparts exhibit three characteristic peaks at about 28.0°, 47.5° and 55.3°, which can be assigned to (112), (024) and (132) lattice plane of tetragonal phase of $Cu_{0.412}In_{0.412}Zn_{0.175}S$ (JCPDS no. 47-1371) [20]. What's more, the diffraction peaks of Zn or Cu decorated In_2S_3 QDs ($ZnIn_2S_4$ or $Cu_{0.4}$-In_2S_3) are well corresponding to that of $Cu_{0.4}$-$ZnIn_2S_4$, demonstrating the identical crystal structure of the above QDs. Additionally, the varied contents of Zn or Cu hardly shifted the diffraction peaks of the as-prepared indium-based chalcogenide QDs (Figure S1), which probably owes to the similar radius of Zn^{2+} (0.74 Å), Cu^{+} (0.74 Å) and In^{3+} (0.76 Å) [28,29], demonstrating the preservation of crystal structure during the transition metal ions decoration.

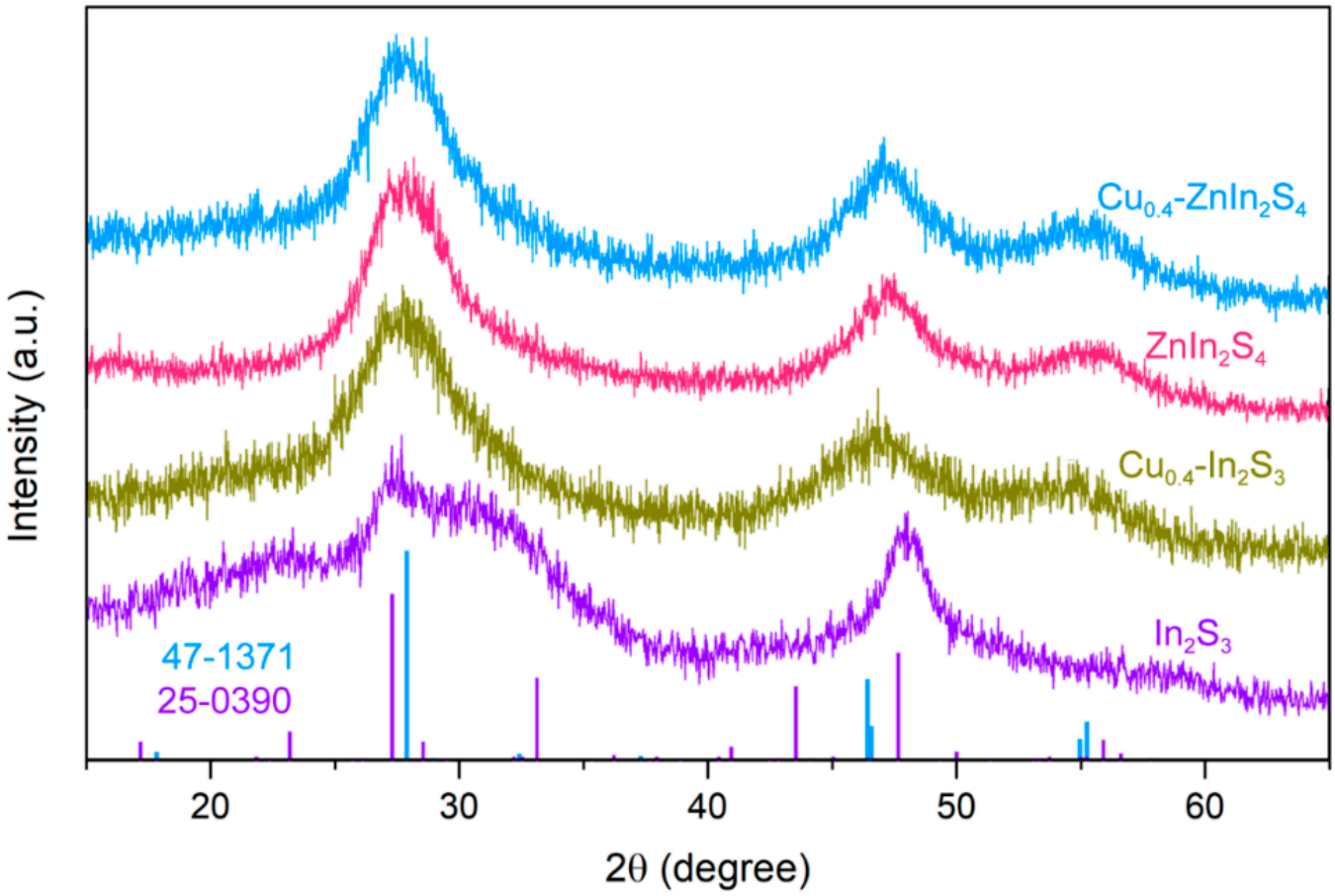

Figure 1. The XRD patterns of In_2S_3, $Cu_{0.4}$-In_2S_3, $ZnIn_2S_4$ and $Cu_{0.4}$-$ZnIn_2S_4$ QDs.

The size and morphology of the synthesized various QDs were also investigated. According to Debye–Scherrer formula, the broad diffraction peaks implied the ultra-small size of the nanocrystals in three dimensions [30,31]. While the similar full width at half maximum (FWHM) of different contents of Zn and/or Cu decorated In_2S_3 QDs indicated the approximate size (Figure 1). It should be mentioned that FWHM of pristine In_2S_3 QDs was smaller than the other QDs, which implied the slightly larger size of In_2S_3 QDs. Indeed, the diameters in terms of XRD patterns for In_2S_3, $Cu_{0.4}$-In_2S_3, $ZnIn_2S_4$ and $Cu_{0.4}$-$ZnIn_2S_4$ QDs along the (024) plane is 3.8 nm, 2.6 nm, 2.6 nm and 3.1 nm, respectively (the difference of size could be ignored in the photocatalytic activity comparison owing to the seriously faint photocatalytic H_2 evolution of In_2S_3 QDs). The diameters of various QDs were further characterized by the transmission electron microscope (TEM) images. As shown in Figure 2a, the In_2S_3 QDs displayed the near-spherical nanocrystals with the diameter of about 3.9 nm, while the other three QDs (Figure 2b–d) were also near-spherical nanocrystals with the diameter ranging from 2.7~3.0 nm, slightly smaller than the pristine In_2S_3 QDs. What's more, the high-resolution TEM (HR-TEM) images revealed that the lattice spacing of all the QDs was 3.1 Å [20,32,33], which was corresponding to the (112) plane of tetragonal phase of In_2S_3, $ZnIn_2S_4$ or their doped counterparts, further demonstrating that the crystal structure of tetragonal phase was well preserved after the introduction of Zn and/or Cu ions into the In_2S_3 QDs.

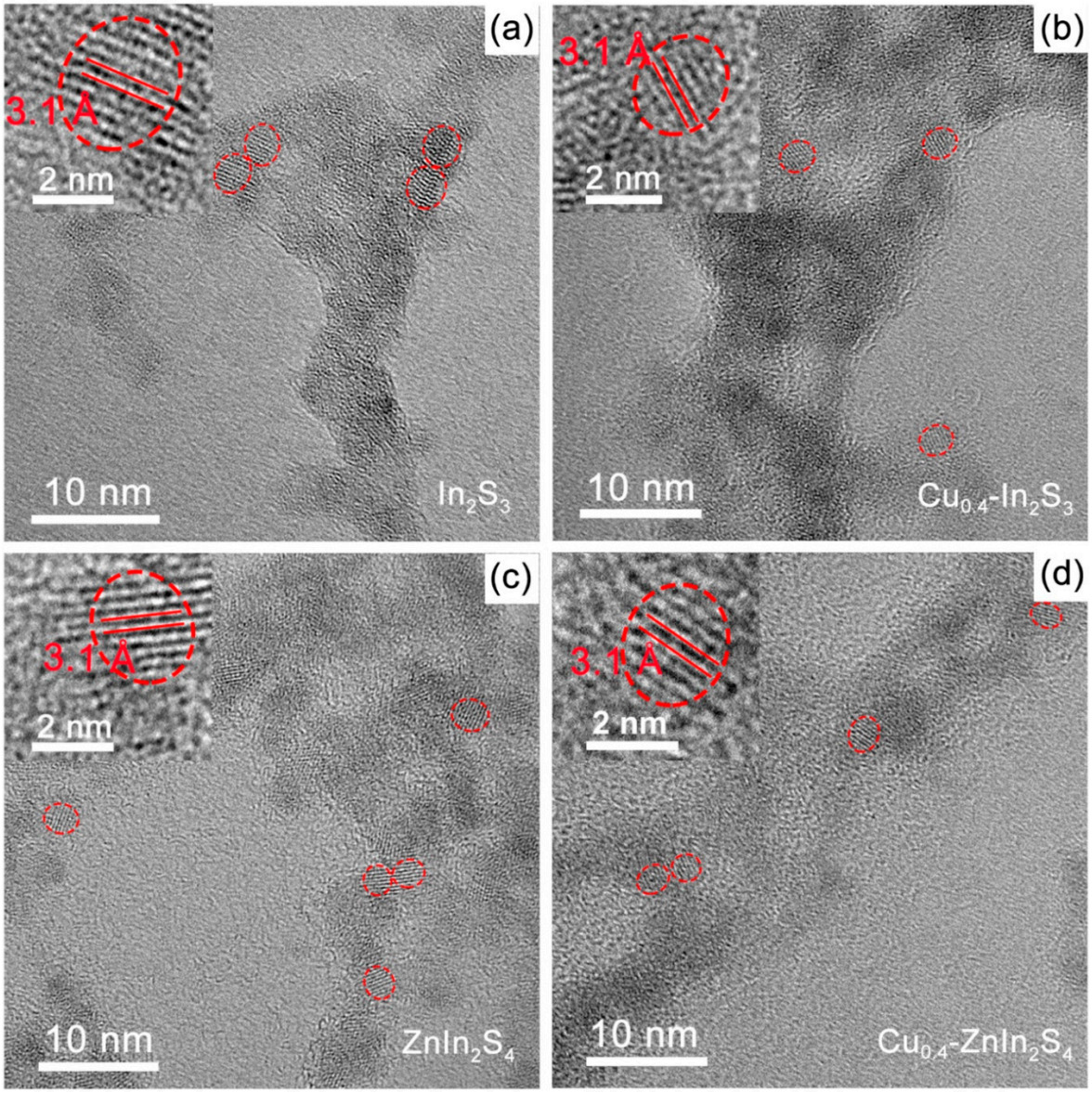

Figure 2. The TEM images of (**a**) In_2S_3, (**b**) $Cu_{0.4}$-In_2S_3, (**c**) $ZnIn_2S_4$ and (**d**) $Cu_{0.4}$-$ZnIn_2S_4$ QDs. The insets show the corresponding high-resolution TEM images.

To gain more insight into the chemical composition and valence state of metal elements in the prepared various QDs, the X-ray photoelectron spectroscopy (XPS) was explored. The peaks of Cu, Zn, In and S elements were clearly observed in the XPS survey spectrum of $Cu_{0.4}$-$ZnIn_2S_4$ QDs [19,34,35], while the In_2S_3, $ZnIn_2S_4$ and $Cu_{0.4}$-In_2S_3 also clearly manifested their respective peaks without the presence of other metal elements (Figure 3a), suggesting the rational chemical composition in the designed QDs. Furthermore, the binding energy of Cu $2p_{3/2}$ and Cu $2p_{1/2}$ in both $Cu_{0.4}$-In_2S_3 and $Cu_{0.4}$-$ZnIn_2S_4$ QDs was at 932.3 eV and 952.1 eV (Figure 3b), suggesting the monovalent Cu in the QDs, which could be further demonstrated by the absence of satellite peak [36]. The decrease of valence state of Cu probably owes to the reduction by L-cysteine. What's more, the binding energies of Zn 2p (1022.1 eV for $2p_{3/2}$ and 1045.2 eV for $2p_{1/2}$) and In 3d (444.6 eV for $3d_{5/2}$ and 452.2 eV for $3d_{3/2}$) in $Cu_{0.4}$-$ZnIn_2S_4$ QDs (Figure 3c,d), suggested that the chemical states of Zn and In are +2 and +3, respectively, which were in good agreement with the previous reports on Zn-In-S ternary semiconductors [37,38]. Additionally, the features and positions of In 3d, Zn 2p and S 2p peaks (Figure 3c,d and Figure S2) remained the same in the four QDs, indicating the similar lactic framework and coordination environment of the indium-

based chalcogenide QDs. Combining all the above results, we believe that by regulating the species and amount of precursors, the Zn and/or Cu decorated In_2S_3 QDs with the identical crystal structure and similar size have been successfully prepared.

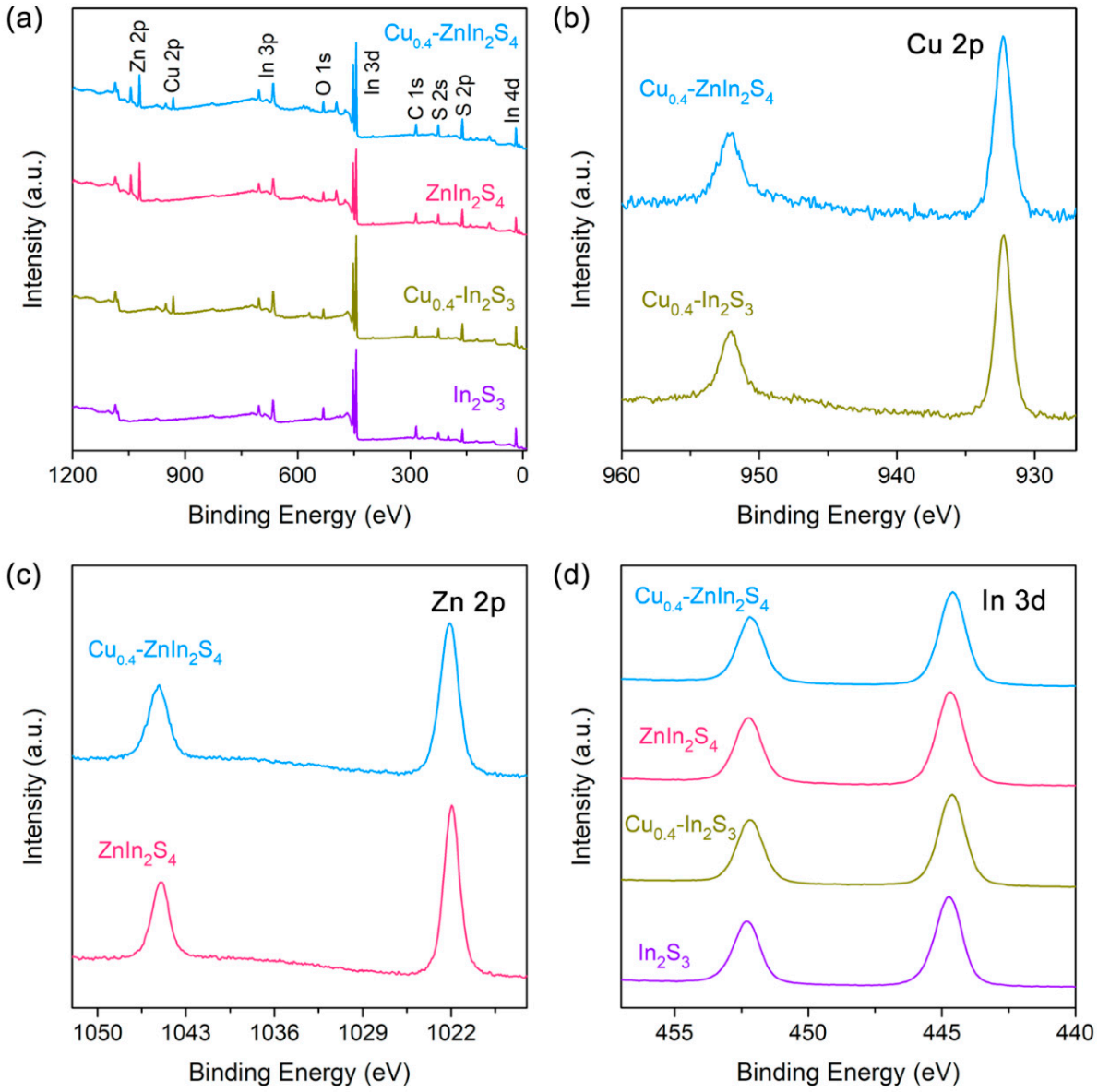

Figure 3. (**a**) The XPS survey spectra of In_2S_3, $Cu_{0.4}$-In_2S_3, $ZnIn_2S_4$ and $Cu_{0.4}$-$ZnIn_2S_4$ QDs. The high-resolution XPS spectra of (**b**) Cu 2p, (**c**) Zn 2p and (**d**) In 3d in various QDs, respectively.

3.2. Photocatalytic H_2 Evolution

The photocatalytic activity of the as-prepared QDs were investigated by using the QDs as absorber and in situ loaded Ni^{2+} as cocatalysts. It indicated that without the introduction of Cu, there was no H_2 to be detected for the $ZnIn_2S_4$ QDs, and only trace amount of H_2 was produced for In_2S_3 QDs under 460 nm LEDs irradiation (Figure 4a). However, the photocatalytic H_2 evolution activity dramatically increased after the doping of Cu for both In_2S_3 and $ZnIn_2S_4$ QDs, probably owing to the outstanding visible light harvesting by the narrowed bandgap. Therefore, the photocatalytic H_2 evolution activities for different contents of Cu decorated QDs were further explored. As shown in Figure S3, the photocatalytic H_2 evolution activity of both Cu-doped In_2S_3 and $ZnIn_2S_4$ QDs increased with the increased Cu contents at first and then decreased. This is due that the introduction

of Cu would decrease the bandgap of QDs, which resulted in the enhanced photocatalytic activity. While the excess introduction of Cu would lead to the decreased redox driving force as well as the formation of Cu defects for non-radiative carrier recombination centers, which was unfavorable for the photocatalytic H_2 evolution.

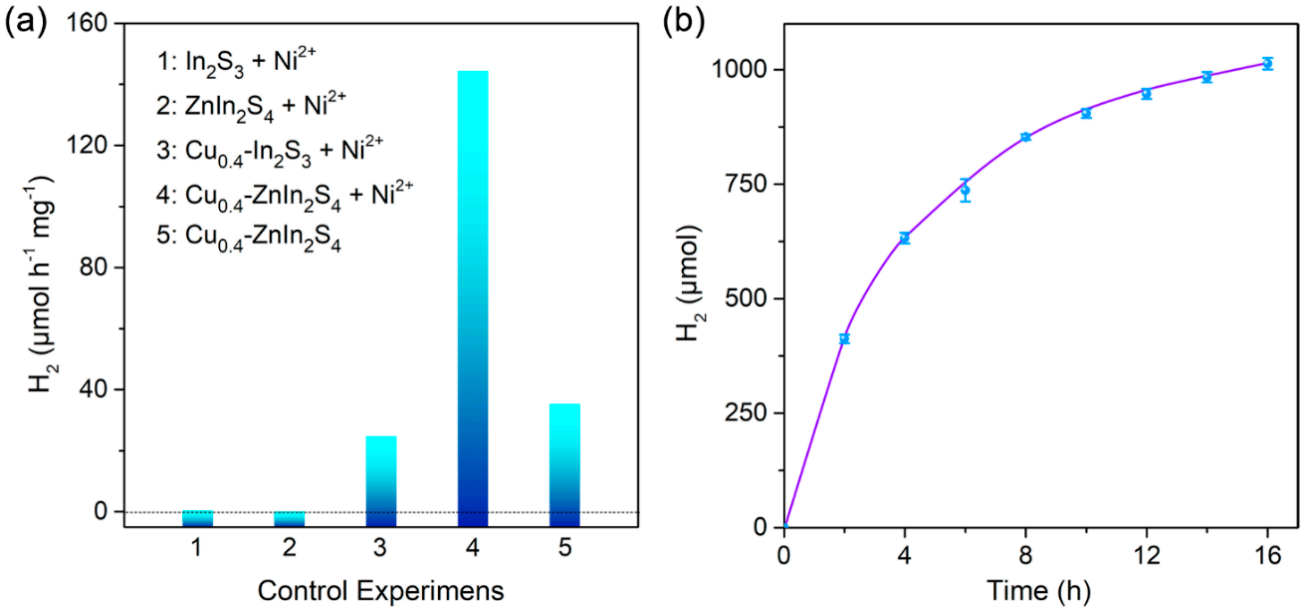

Figure 4. (**a**) Comparison of H_2 evolution of $Cu_{0.4}$-$ZnIn_2S_4$ QDs with In_2S_3, $ZnIn_2S_4$ and $Cu_{0.4}$-In_2S_3 QDs under the in situ loaded Ni^{2+} as cocatalysts, and photocatalytic activity comparison of $Cu_{0.4}$-$ZnIn_2S_4$ QDs with/without cocatalysts. (**b**) Long-time photocatalytic H_2 evolution of $Cu_{0.4}$-$ZnIn_2S_4$ QDs under optimal conditions. The photocatalytic reaction was performed with 1.6 mg of QDs, 10 μg of nickel acetate tetrahydrate and 400 mg of ascorbic acid dispersed in 6.0 mL aqueous solution at pH 5.2, using 460 nm LEDs irradiation. Error bars represent the mean ± s.d. of multiple independent experiments.

The photocatalytic H_2 evolution rate for optimal Cu-doped $ZnIn_2S_4$ ($Cu_{0.4}$-$ZnIn_2S_4$) QDs could reach to 144.4 μmol h^{-1} mg^{-1}, which was nearly 480-fold and 6-fold higher than that of pristine In_2S_3 and $Cu_{0.4}$-In_2S_3 QDs under identical conditions respectively (Figure 4a), implying the significant impact of Zn introduction for the enhancement of photocatalytic performance. Apparently, the photocatalytic H_2 evolution rate is even comparable to the state-of-the-art cadmium chalcogenides QDs [26,39]. Control experiments also demonstrated that without the Ni^{2+}, the photocatalytic activity would decrease by three fourths, indicated the vital role of cocatalysts. Long-time H_2 evolution performance of the $Cu_{0.4}$-$ZnIn_2S_4$ QDs was also examined under optimal conditions. As shown in Figure 4b, the rate was decreased with the irradiation time probably owing to the photocurrosion, however, ~1013 μmol of H_2 could be obtained from 6.0 mL aqueous solution within 16 h irradiation, giving the TON of 20260 per QD. And the AQY of $Cu_{0.4}$-$ZnIn_2S_4$ QDs could reach 11.8% at 460 nm.

3.3. Mechanism for Photocatalytic H_2 Production

To shed light on the effect of the introduction of transition metal ions, the UV-visible absorption spectra of various QDs were carried out. As shown in Figure 5a, the In_2S_3 QDs exhibited faint absorption for visible light, which was corresponding to their negligible photocatalytic activity. As the intrinsic bandgap of bulk In_2S_3 is 2.3 eV [40–42], the faint visible light absorption of the as-prepared In_2S_3 QDs was mainly owing to broadening bandgap resulted by the quantum confinement effect. Further investigation indicated that the introduction of Zn and Cu elements played the opposite effect for the In_2S_3 QDs [43]. The absorption onset of $ZnIn_2S_4$ QDs was less than 400 nm, implied the broader bandgap after the introduction of Zn. However, the Cu-doped In_2S_3 QDs displayed the robust visible

light harvesting and the absorption tail could rise up to 700 nm, implied the narrower bandgap. What's more, the doping of Cu would also narrow the bandgap of $ZnIn_2S_4$ QDs, and the absorption onset of $Cu_{0.4}$-$ZnIn_2S_4$ QDs redshifted to 600 nm [44]. Therefore, the introduction of Cu makes the main contribution for the bandgap narrowing.

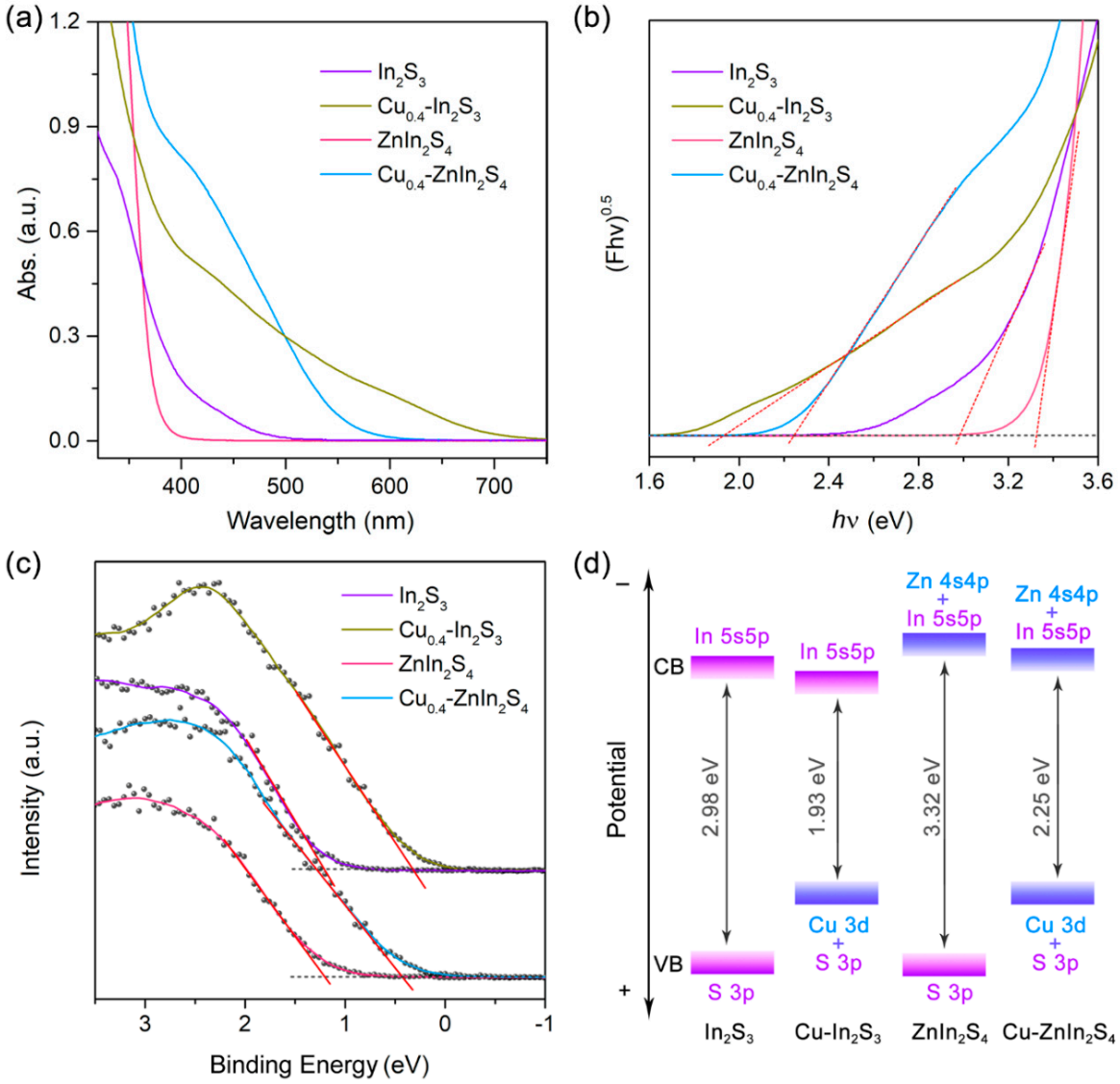

Figure 5. (**a**) The UV- vis absorption spectra, (**b**) corresponding Tauc plots, (**c**) XPS valence band spectra and (**d**) the corresponding band position alignment of In_2S_3, $Cu_{0.4}$-In_2S_3, $ZnIn_2S_4$ and $Cu_{0.4}$-$ZnIn_2S_4$ QDs.

Although the optical density of $Cu_{0.4}$-$ZnIn_2S_4$ was slightly higher than that of $Cu_{0.4}$-In_2S_3 at 460 nm (Figure 5a), the difference of absorption ability hardly resulted in the 6-fold enhancement of photocatalytic activity. Therefore, the band positions of the four QDs were further investigated by Tauc plot and XPS valence band spectra. Figure 5b revealed that the bandgap of In_2S_3, $ZnIn_2S_4$ and their Cu-doped counterparts were 2.98 eV, 3.32 eV, 1.93 eV and 2.25 eV, respectively, which was consistent with the results of absorption spectra. While the valence band edges of In_2S_3 and $ZnIn_2S_4$ were close, at 1.20 V and 1.22 V (vs. NHE) respectively (Figure 5c), which was owing that the valence band of the chalcogenide semiconductors were mainly composed by S 3p orbitals [45]. However, the introduction of Cu ions would create a Cu dopant level above the pristine valence band edge [3,46], causing their obvious upshift (*ca.* 0.8 V). Combined with the difference in bandgap, the conduction band edges of In_2S_3 and $ZnIn_2S_4$ could be calculated at −1.78 V and −2.10 V,

indicated the 0.32 V upshift after the introduction of Zn, which could also be observed for the comparison of $Cu_{0.4}$-In_2S_3 and $Cu_{0.4}$-$ZnIn_2S_4$ (Figure 5d). This is because that the conduction band minimum is mainly composed of hybrid d and sp orbitals of the metal cations [47], therefore, the introduction of Zn would result in the change of conduction band from In 5s5p to more negative hybrid orbitals of In 5s5p and Zn 4s4p [46,48]. The upshift of the conduction band edges gave rise to a higher thermodynamic driving force of proton reduction, and hence remarkably accelerating the H_2 evolution rate in water splitting.

Next, we employed the steady-state emission quenching experiments to evaluate the charge transfer process. Take the $Cu_{0.4}$-$ZnIn_2S_4$ QDs as example, excitation of QDs at 430 nm would result in strong luminescence at 630 nm (Figure 6a), which roughly corresponded to the bandgap energy of $Cu_{0.4}$-$ZnIn_2S_4$ QDs, indicating that this is the band edge emission of $Cu_{0.4}$-$ZnIn_2S_4$ QDs. However, the emission intensity was dramatically quenched with the adding of Ni^{2+} (Figure 6a), indicating that the binding of Ni^{2+} with the QDs would result in the electron transfer from the QDs to Ni^{2+} and consequently inhibit the radiative recombination of photogenerated electron-hole pairs [49]. What's more, after adding electron donor, H_2A, into the QDs aqueous solution, the emission would also be quenched obviously (Figure 6b), demonstrating the hole transfer from QDs to H_2A [50].

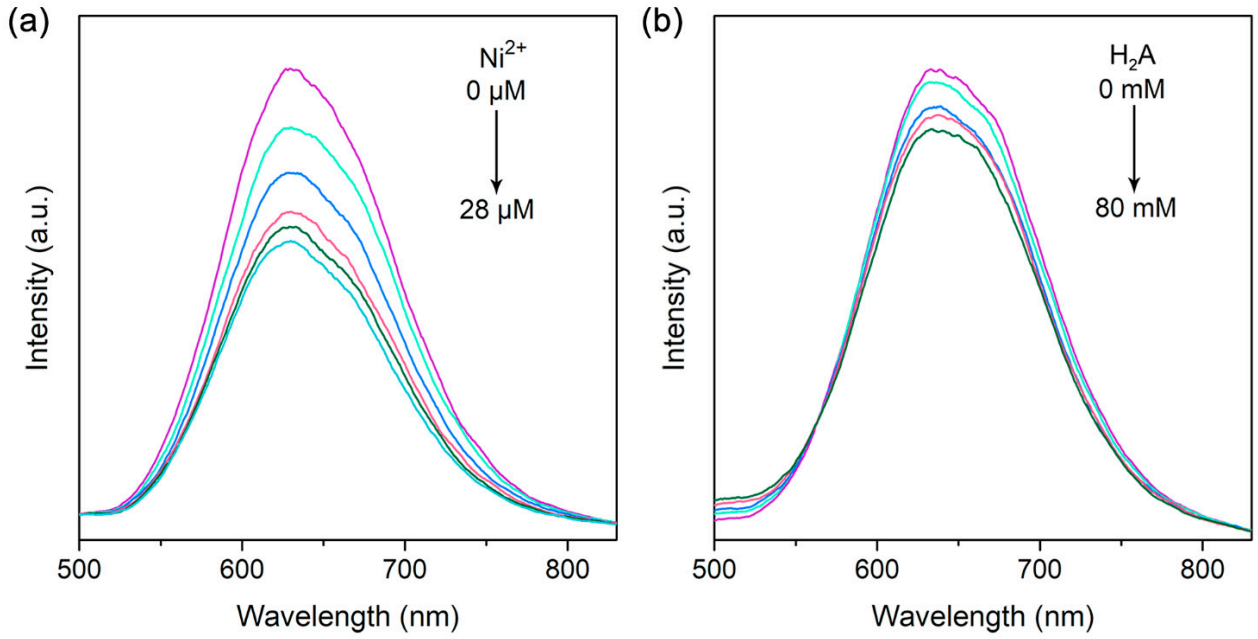

Figure 6. Steady-state emission quenching of $Cu_{0.4}$-$ZnIn_2S_4$ QDs with gradual addition of (**a**) Ni^{2+} and (**b**) H_2A.

On the basis of the above results, we proposed that the introduction of Zn and Cu ions would regulate the conduction and valence band of indium chalcogenide QDs, respectively. As the upshift of valence band edge was significantly larger than that of conduction band edge, the bandgap of Cu doped QDs was clearly narrowed and gave rise to the robust visible light harvesting. Therefore, the photocatalytic activity of QDs remarkably enhanced after the doping of Cu. On the other hand, with the upshift of the conduction band edge, the thermodynamic driving force of proton reduction raised, thus the Cu-doped $ZnIn_2S_4$ QDs exhibited the superior photocatalytic activity. Under visible light irradiation, the photogenerated electron of $Cu_{0.4}$-$ZnIn_2S_4$ QDs would transfer to the surface Ni species, the H_2 evolution cocatalysts, which would assist the proton reduction and formation of H_2. Simultaneously, the hole transferred to the surface of QDs and oxidized the electron donor to accomplish the whole reaction (Figure 7).

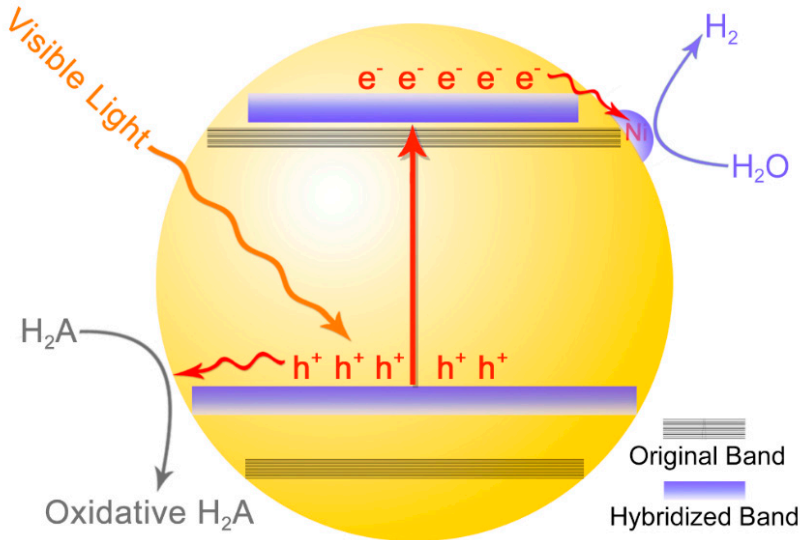

Figure 7. The transformation of conduction/valence band of In_2S_3 QDs after the decoration of Zn and Cu, as well as the photocatalytic H_2 evolution mechanism of the $Cu_{0.4}$-$ZnIn_2S_4$ QDs.

4. Conclusions

In summary, we have regulated the bandgap and conduction/valence band levels of indium-based chalcogenides QDs simultaneously by introducing transition metal ions to construct efficient and noble metal-free photocatalysts. The bandgap is mainly determined by the doping of Cu, which could remarkably upshift the valence band edge. While the introduction of Zn would slightly enhance the conduction band level and provide higher driving force for proton reduction. Therefore, the as-prepared Cu-doped $ZnIn_2S_4$ QDs exhibit outstandingly higher photocatalytic performance. Under the optimal conditions, the $Cu_{0.4}$-$ZnIn_2S_4$ QDs could produce H_2 with the rate of 144.4 μmol h^{-1} mg^{-1}, which is even comparable to the state-of-the-art cadmium chalcogenide QDs. We believe that this approach has given a much deeper recognition on the band engineering, which can be extended to related systems as an effective strategy for the design of photocatalysts.

Supplementary Materials: The following are available online at https://www.mdpi.com/article/10.3390/nano11051115/s1, Table S1: Comparison of photocatalytic H_2 evolution with reported cadmium chalcogenide QDs-based systems; Figure S1: The XRD patterns of Cu-doped Zn-In-S QDs (the ratio in the graph represents the molar ratio of Cu:Zn:In); Figure S2: The high-resolution XPS spectra of S 2p of In_2S_3, $Cu_{0.4}$-In_2S_3, $ZnIn_2S_4$ and $Cu_{0.4}$-$ZnIn_2S_4$ QDs; Figure S3: The photocatalytic H_2 evolution comparison of different contents of Cu doped (a) In_2S_3 and (b) $ZnIn_2S_4$ QDs.

Author Contributions: Conceptualization, Y.-J.G.; methodology, X.-P.L. and R.-J.H.; validation, Y.-J.G. and C.C.; formal analysis, X.-P.L. and Y.-J.G.; investigation, X.-P.L. and R.-J.H.; resources, Y.-J.G. and T.L.; data curation, X.-P.L. and Y.-J.G.; writing—original draft preparation, X.-P.L.; writing—review and editing, Y.-J.G.; visualization, Y.-J.G. and T.L.; supervision, T.L.; project administration, Y.-J.G.; funding acquisition, Y.-J.G. All authors have read and agreed to the published version of the manuscript.

Funding: This work was supported by National Natural Science Foundation of China (22002065, 21776143), Natural Science Foundation of Shandong Province (ZR2020QB060), Program for Scientific Research Innovation Team in Colleges and Universities of Shandong Province, Key Laboratory of Photochemical Conversion and Optoelectronic Materials, Technical Institute of Physics and Chemistry, CAS (PCOM201914).

Data Availability Statement: The data presented in this study are available on request from the corresponding author.

Conflicts of Interest: The authors declare no conflict of interest.

References

1. Wang, Z.; Li, C.; Domen, K. Recent developments in heterogeneous photocatalysts for solar-driven overall water splitting. *Chem. Soc. Rev.* **2019**, *48*, 2109–2125. [CrossRef]
2. Gong, J.; Li, C.; Wasielewski, M.R. Advances in solar energy conversion. *Chem. Soc. Rev.* **2019**, *48*, 1862–1864. [CrossRef]
3. Chandrasekaran, S.; Yao, L.; Deng, L.; Bowen, C.; Zhang, Y.; Chen, S.; Lin, Z.; Peng, F.; Zhang, P. Recent advances in metal sulfides: From controlled fabrication to electrocatalytic, photocatalytic and photoelectrochemical water splitting and beyond. *Chem. Soc. Rev.* **2019**, *48*, 4178–4280. [CrossRef]
4. Reisner, E. When Does Organic Photoredox Catalysis Meet Artificial Photosynthesis? *Angew. Chem. Int. Ed.* **2019**, *58*, 3656–3657. [CrossRef]
5. Kim, J.H.; Hansora, D.; Sharma, P.; Jang, J.-W.; Lee, J.S. Toward practical solar hydrogen production—An artificial photosynthetic leaf-to-farm challenge. *Chem. Soc. Rev.* **2019**, *48*, 1908–1971. [CrossRef]
6. Li, X.-B.; Xin, Z.-K.; Xia, S.-G.; Gao, X.-Y.; Tung, C.-H.; Wu, L.-Z. Semiconductor nanocrystals for small molecule activation via artificial photosynthesis. *Chem. Soc. Rev.* **2020**, *49*, 9028–9056. [CrossRef] [PubMed]
7. Kundu, S.; Patra, A. Nanoscale Strategies for Light Harvesting. *Chem. Rev.* **2017**, *117*, 712–757. [CrossRef] [PubMed]
8. Su, D.W.; Ran, J.; Zhuang, Z.W.; Chen, C.; Qiao, S.Z.; Li, Y.D.; Wang, G.X. Atomically dispersed Ni in cadmium-zinc sulfide quantum dots for high-performance visible-light photocatalytic hydrogen production. *Sci. Adv.* **2020**, *6*, eaaz8447. [CrossRef] [PubMed]
9. Kodaimati, M.S.; Lian, S.; Schatz, G.C.; Weiss, E.A. Energy transfer-enhanced photocatalytic reduction of protons within quantum dot light-harvesting–catalyst assemblies. *Proc. Natl. Acad. Sci. USA* **2018**, *115*, 8290–8295. [CrossRef]
10. Li, X.-B.; Gao, Y.-J.; Wang, Y.; Zhan, F.; Zhang, X.-Y.; Kong, Q.-Y.; Zhao, N.-J.; Guo, Q.; Wu, H.-L.; Li, Z.-J.; et al. Self-Assembled Framework Enhances Electronic Communication of Ultrasmall-Sized Nanoparticles for Exceptional Solar Hydrogen Evolution. *J. Am. Chem. Soc.* **2017**, *139*, 4789–4796. [CrossRef]
11. Chava, R.K.; Son, N.; Kim, Y.S.; Kang, M. Controlled Growth and Bandstructure Properties of One Dimensional Cadmium Sulfide Nanorods for Visible Photocatalytic Hydrogen Evolution Reaction. *Nanomaterials* **2020**, *10*, 619. [CrossRef]
12. Luo, N.; Montini, T.; Zhang, J.; Fornasiero, P.; Fonda, E.; Hou, T.; Nie, W.; Lu, J.; Liu, J.; Heggen, M.; et al. Visible-light-driven coproduction of diesel precursors and hydrogen from lignocellulose-derived methylfurans. *Nat. Energy* **2019**, *4*, 575–584. [CrossRef]
13. Li, X.; Sun, Y.; Xu, J.; Shao, Y.; Wu, J.; Xu, X.; Pan, Y.; Ju, H.; Zhu, J.; Xie, Y. Selective visible-light-driven photocatalytic CO_2 reduction to CH_4 mediated by atomically thin $CuIn_5S_8$ layers. *Nat. Energy* **2019**, *4*, 690–699. [CrossRef]
14. Pan, X.; Shang, C.; Chen, Z.; Jin, M.; Zhang, Y.; Zhang, Z.; Wang, X.; Zhou, G. Enhanced Photocatalytic H_2 Evolution over $ZnIn_2S_4$ Flower-Like Microspheres Doped with Black Phosphorus Quantum Dots. *Nanomaterials* **2019**, *9*, 1266. [CrossRef]
15. Sharma, R.K.; Chouryal, Y.N.; Chaudhari, S.; Saravanakumar, J.; Dey, S.R.; Ghosh, P. Adsorption-Driven Catalytic and Photocatalytic Activity of Phase Tuned In_2S_3 Nanocrystals Synthesized via Ionic Liquids. *ACS Appl. Mater. Interfaces* **2017**, *9*, 11651–11661. [CrossRef]
16. Gao, Y.-J.; Li, X.-B.; Wang, X.-Z.; Zhao, N.-J.; Zhao, Y.; Wang, Y.; Xin, Z.-K.; Zhang, J.-P.; Zhang, T.; Tung, C.-H.; et al. Site- and Spatial-Selective Integration of Non-noble Metal Ions into Quantum Dots for Robust Hydrogen Photogeneration. *Matter* **2020**, *3*, 571–585. [CrossRef]
17. Das, A.; Han, Z.; Haghighi, M.G.; Eisenberg, R. Photogeneration of hydrogen from water using CdSe nanocrystals demonstrating the importance of surface exchange. *Proc. Natl. Acad. Sci. USA* **2013**, *110*, 16716–16723. [CrossRef] [PubMed]
18. Wang, Y.; Ma, Y.; Li, X.-B.; Gao, L.; Gao, X.-Y.; Wei, X.-Z.; Zhang, L.-P.; Tung, C.-H.; Qiao, L.; Wu, L.-Z. Unveiling Catalytic Sites in a Typical Hydrogen Photogeneration System Consisting of Semiconductor Quantum Dots and 3d-metal Ions. *J. Am. Chem. Soc.* **2020**, *142*, 4680–4689. [CrossRef]
19. Fan, X.-B.; Yu, S.; Zhan, F.; Li, Z.-J.; Gao, Y.-J.; Li, X.-B.; Zhang, L.-P.; Tao, Y.; Tung, C.-H.; Wu, L.-Z. Nonstoichiometric Cu_xIn_yS Quantum Dots for Efficient Photocatalytic Hydrogen Evolution. *ChemSusChem* **2018**, *10*, 4833–4838. [CrossRef]
20. Tan, L.; Liu, Y.; Mao, B.; Luo, B.; Gong, G.; Hong, Y.; Chen, B.; Shi, W. Effective bandgap narrowing of Cu–In–Zn–S quantum dots for photocatalytic H_2 production via cocatalyst-alleviated charge recombination. *Inorg. Chem. Front.* **2018**, *5*, 258–265. [CrossRef]
21. Ramasamy, K.; Shinde, P.S.; Naghibolashrafi, N.; Pan, S.; Gupta, A. Nanocrystals of $CuMSnS_4$ (M = In or Ga) for solar energy conversion applications. *Chem. Commun.* **2018**, *54*, 11757–11760. [CrossRef]
22. Gong, G.; Liu, Y.; Mao, B.; Tan, L.; Yang, Y.; Shi, W. Ag doping of Zn-In-S quantum dots for photocatalytic hydrogen evolution: Simultaneous bandgap narrowing and carrier lifetime elongation. *Appl. Catal. B* **2017**, *216*, 11–19. [CrossRef]
23. Wu, K.; Lian, T. Quantum confined colloidal nanorod heterostructures for solar-to-fuel conversion. *Chem. Soc. Rev.* **2016**, *45*, 3781–3810. [CrossRef]
24. Du, J.; Du, Z.; Hu, J.-S.; Pan, Z.; Shen, Q.; Sun, J.; Long, D.; Dong, H.; Sun, L.; Zhong, X.; et al. Zn–Cu–In–Se Quantum Dot Solar Cells with a Certified Power Conversion Efficiency of 11.6%. *J. Am. Chem. Soc.* **2016**, *138*, 4201–4209. [CrossRef] [PubMed]
25. Moniz, S.J.A.; Shevlin, S.A.; Martin, D.J.; Guo, Z.-X.; Tang, J. Visible-light driven heterojunction photocatalysts for water splitting—A critical review. *Energy Environ. Sci.* **2015**, *8*, 731–759. [CrossRef]
26. Li, X.-B.; Tung, C.-H.; Wu, L.-Z. Semiconducting quantum dots for artificial photosynthesis. *Nat. Rev. Chem.* **2018**, *2*, 160–173. [CrossRef]

27. Li, H.; Gao, Y.; Zhou, Y.; Fan, F.; Han, Q.; Xu, Q.; Wang, X.; Xiao, M.; Li, C.; Zou, Z. Construction and Nanoscale Detection of Interfacial Charge Transfer of Elegant Z-Scheme WO_3/Au/In_2S_3 Nanowire Arrays. *Nano Lett.* **2016**, *16*, 5547–5552. [CrossRef]
28. Pan, D.; An, L.; Sun, Z.; Hou, W.; Yang, Y.; Yang, Z.; Lu, Y. Synthesis of Cu−In−S Ternary Nanocrystals with Tunable Structure and Composition. *J. Am. Chem. Soc.* **2008**, *130*, 5620–5621. [CrossRef]
29. Wang, J.; Li, G.; Li, Z.; Tang, C.; Feng, Z.; An, H.; Liu, H.; Liu, T.; Li, C. A highly selective and stable ZnO-ZrO_2 solid solution catalyst for CO_2 hydrogenation to methanol. *Sci. Adv.* **2017**, *3*, 1701290. [CrossRef]
30. Tian, H.; Zhang, X.L.; Scott, J.; Ng, C.; Amal, R. TiO_2-Supported Copper Nanoparticles Prepared via Ion Exchange for Photocatalytic Hydrogen Production. *J. Mater. Chem. A* **2014**, *2*, 6432–6438. [CrossRef]
31. Robinson, R.D.; Sadtler, B.; Demchenko, D.O.; Erdonmez, C.K.; Wang, L.-W.; Alivisatos, A.P. Spontaneous Superlattice Formation in Nanorods Through Partial Cation Exchange. *Science* **2007**, *317*, 355–358. [CrossRef]
32. Yuan, Y.-J.; Chen, D.-Q.; Huang, Y.-W.; Yu, Z.-T.; Zhong, J.-S.; Chen, T.-T.; Tu, W.-G.; Guan, Z.-J.; Cao, D.-P.; Zou, Z.-G. MoS_2 Nanosheet-Modified $CuInS_2$ Photocatalyst for Visible-Light-Driven Hydrogen Production from Water. *ChemSusChem* **2016**, *9*, 1003–1009. [CrossRef] [PubMed]
33. Zhang, Z.; Huang, L.; Zhang, J.; Wang, F.; Xie, Y.; Shang, X.; Gu, Y.; Zhao, H.; Wang, X. In situ constructing interfacial contact MoS_2/$ZnIn_2S_4$ heterostructure for enhancing solar photocatalytic hydrogen evolution. *Appl. Catal. B* **2018**, *233*, 112–119. [CrossRef]
34. Zeng, C.; Huang, H.; Zhang, T.; Dong, F.; Zhang, Y.; Hu, Y. Fabrication of Heterogeneous-Phase Solid-Solution Promoting Band Structure and Charge Separation for Enhancing Photocatalytic CO_2 Reduction: A Case of $Zn_XCa_{1-X}In_2S_4$. *ACS Appl. Mater. Interfaces* **2017**, *9*, 27773–27783. [CrossRef]
35. Li, X.-L.; Wang, X.-J.; Zhu, J.-Y.; Li, Y.-P.; Zhao, J.; Li, F.-T. Fabrication of two-dimensional Ni_2P/$ZnIn_2S_4$ heterostructures for enhanced photocatalytic hydrogen evolution. *Chem. Eng. J.* **2018**, *353*, 15–24. [CrossRef]
36. Chen, Y.; Zhao, S.; Wang, X.; Peng, Q.; Lin, R.; Wang, Y.; Shen, R.; Cao, X.; Zhang, L.; Zhou, G.; et al. Synergetic Integration of $Cu_{1.94}S$–$Zn_xCd_{1-x}S$ Heteronanorods for Enhanced Visible-Light-Driven Photocatalytic Hydrogen Production. *J. Am. Chem. Soc.* **2016**, *138*, 4286–4289. [CrossRef]
37. Zhang, S.; Liu, X.; Liu, C.; Luo, S.; Wang, L.; Cai, T.; Zeng, Y.; Yuan, J.; Dong, W.; Pei, Y.; et al. MoS_2 Quantum Dot Growth Induced by S Vacancies in a $ZnIn_2S_4$ Monolayer: Atomic-Level Heterostructure for Photocatalytic Hydrogen Production. *ACS Nano* **2018**, *12*, 751–758. [CrossRef]
38. Xing, F.; Liu, Q.; Huang, C. Mo-Doped $ZnIn_2S_4$ Flower-Like Hollow Microspheres for Improved Visible Light-Driven Hydrogen Evolution. *Solar RRL* **2020**, *4*, 1900483. [CrossRef]
39. Gao, Y.-J.; Li, X.-B.; Wu, H.-L.; Meng, S.-L.; Fan, X.-B.; Huang, M.-Y.; Guo, Q.; Tung, C.-H.; Wu, L.-Z. Exceptional Catalytic Nature of Quantum Dots for Photocatalytic Hydrogen Evolution without External Cocatalysts. *Adv. Funct. Mater.* **2018**, *28*, 1801769. [CrossRef]
40. Lai, P.-Y.; Huang, C.-C.; Chou, T.-H.; Ou, K.-L.; Chang, J.-Y. Aqueous synthesis of Ag and Mn co-doped In_2S_3/ZnS quantum dots with tunable emission for dual-modal targeted imaging. *Acta Biomater.* **2017**, *50*, 522–533. [CrossRef]
41. Ning, J.; Men, K.; Xiao, G.; Zhao, L.; Wang, L.; Liu, B.; Zou, B. Synthesis, optical properties and growth process of In_2S_3 nanoparticles. *J. Colloid Interface Sci.* **2010**, *347*, 172–176. [CrossRef] [PubMed]
42. Shen, S.; Wang, Q. Rational Tuning the Optical Properties of Metal Sulfide Nanocrystals and Their Applications. *Chem. Mater.* **2012**, *25*, 1166–1178. [CrossRef]
43. Kim, J.; Wong, C.Y.; Scholes, G.D. Exciton Fine Structure and Spin Relaxation in Semiconductor Colloidal Quantum Dots. *Acc. Chem. Res.* **2009**, *42*, 1037–1046. [CrossRef] [PubMed]
44. Kershaw, S.V.; Susha, A.S.; Rogach, A.L. Narrow bandgap colloidal metal chalcogenide quantum dots: Synthetic methods, heterostructures, assemblies, electronic and infrared optical properties. *Chem. Soc. Rev.* **2013**, *42*, 3033–3087. [CrossRef] [PubMed]
45. Wang, Y.; Suzuki, H.; Xie, J.; Tomita, O.; Martin, D.J.; Higashi, M.; Kong, D.; Abe, R.; Tang, J. Mimicking Natural Photosynthesis: Solar to Renewable H_2 Fuel Synthesis by Z-Scheme Water Splitting Systems. *Chem. Rev.* **2018**, *118*, 5201–5241. [CrossRef] [PubMed]
46. Hu, P.; Pramana, S.S.; Cao, S.; Ngaw, C.K.; Lin, J.; Loo, S.C.J.; Tan, T.T.Y. Ion-Induced Synthesis of Uniform Single-Crystalline Sulphide-Based Quaternary-Alloy Hexagonal Nanorings for Highly Efficient Photocatalytic Hydrogen Evolution. *Adv. Mater.* **2013**, *25*, 2567–2572. [CrossRef]
47. Chen, S.; Takata, T.; Domen, K. Particulate photocatalysts for overall water splitting. *Nat. Rev. Mater.* **2017**, *2*, 17050. [CrossRef]
48. Kameyama, T.; Takahashi, T.; Machida, T.; Kamiya, Y.; Yamamoto, T.; Kuwabata, S.; Torimoto, T. Controlling the Electronic Energy Structure of ZnS–$AgInS_2$ Solid Solution Nanocrystals for Photoluminescence and Photocatalytic Hydrogen Evolution. *J. Phys. Chem. C* **2015**, *119*, 24740–24749. [CrossRef]
49. Li, Z.-J.; Li, X.-B.; Wang, J.-J.; Yu, S.; Li, C.-B.; Tung, C.-H.; Wu, L.-Z. A robust "artificial catalyst" in situ formed from CdTe QDs and inorganic cobalt salts for photocatalytic hydrogen evolution. *Energy Environ. Sci.* **2013**, *6*, 465–469. [CrossRef]
50. Wang, F.; Liang, W.-J.; Jian, J.-X.; Li, C.-B.; Chen, B.; Tung, C.-H.; Wu, L.-Z. Exceptional Poly(acrylic acid)-Based Artificial [FeFe]-Hydrogenases for Photocatalytic H_2 Production in Water. *Angew. Chem. Int. Ed.* **2013**, *52*, 8134–8138. [CrossRef]